The Effects of Disequilibrium and Deformation on the Mineralogical Evolution of Quartz Diorite During Metamorphism in the Eclogite Facies

by P. O. KOONS*, D. C. RUBIE† AND G. FRUEH-GREEN

Department für Erdwissenschaften, ETH-Zentrum, CH-8092 Zürich, Switzerland

(*Received 14 April 1986; revised typescript accepted 17 February 1987*)

ABSTRACT

In the Sesia Zone, Western Alps, a large volume of orthogneiss formed as a result of eclogite facies metamorphism and deformation of quartz diorite during early Alpine underthrusting and subduction. Rare lenses of undeformed metaquartz diorite, preserved within the orthogneiss, represent an early stage in the evolution of this latter rock type. The metamorphic and microstructural evolution of the orthogneiss in the eclogite facies has been reconstructed from studies of gradational contacts between undeformed and strongly deformed rocks.

High pressure transformations of the original igneous plagioclase + biotite + quartz assemblage to jadeitic pyroxene ($Jd_{0.95-0.85}$) + zoisite + quartz + garnet + 2 muscovites developed prior to deformation. Slow intergranular diffusion resulted in a state of disequilibrium between small textural domains in the metaquartz diorite. The compositions of the phases of the undeformed metaquartz diorite do not reflect the bulk rock composition, but were controlled by their position relative to reactant phases. The jadeitic pyroxenes, for example, formed in localized domains which originally consisted of sodic plagioclase whereas omphacite was the equilibrium pyroxene for the bulk rock composition.

Mineralogical changes which occurred during subsequent deformation of the metaquartz diorite are interpreted as resulting from a progressive enlargement of equilibrium domains and the partial equilibration of mineral compositions to the bulk rock composition rather than from changes in pressure and temperature. Initially during high-strain deformation, fine-grained aggregates of jadeitic pyroxene + quartz + zoisite (originally pseudomorphing plagioclase) are inferred to have deformed by a mechanism of grain boundary sliding accommodated by diffusive mass transfer. Muscovite and garnet compositions homogenized during the deformation but due to slow intracrystalline diffusion, pyroxene compositions ($Jd_{0.95-0.80}$) remained metastable. The coarsening of pyroxene eventually terminated deformation by grain boundary sliding and this mineral subsequently deformed by intracrystalline plasticity. This latter process was accompanied by and perhaps catalysed a change in pyroxene composition from metastable jadeite towards omphacite by a reaction involving the resorption of garnet and the nucleation and growth of paragonite. The resulting orthogneiss consists of quartz + omphacite + garnet + phengite + paragonite + zoisite. The rock is characterized by a broad range of pyroxene compositions ($Jd_{0.8-0.5}$) due to the incomplete equilibration of this mineral to the bulk rock composition and a lack of Fe–Mg exchange equilibrium between pyroxene and garnet. However, in contrast to the undeformed metaquartz diorite, there are no obvious textural indications of disequilibrium between phases in the orthogneiss.

INTRODUCTION

A common aim of metamorphic petrology is to estimate conditions of pressure (P), temperature (T) and fluid composition at which the mineral assemblage of a rock approached or achieved equilibrium. Determination of pressure and temperature is generally

*Present address: Department of Geology, University of Otago, Dunedin, New Zealand.
†Present address: Department of Geology, University of Manchester, Manchester M13 9PL, UK.

based on the assumption that equilibrium among minerals in an assemblage was reached at certain 'peak' metamorphic conditions. The assumption that coexisting minerals represent such an equilibrium assemblage on a thin section scale requires that mineral assemblage equilibration rates are fast compared with rates of change of the state variables until the so called 'peak' conditions are achieved, at which point the equilibration rates must become comparatively slow in order that the record of equilibrium be preserved (see also Spear *et al.* 1982, p. 105). However, many examples have been documented in which the reaction rates were clearly slow compared with rates of change of the physical conditions, even when the temperature of metamorphism exceeded 800 °C (e.g., Loomis, 1976; Tracy & McLellan, 1985). Low reaction rates result in incomplete reactions and disequilibrium, and have been recognized in studies of mineral chemistry and reaction textures (Griffin & Raheim 1973; Loomis, 1976; Mørk, 1985; Tracy & McLellan, 1985). The occurrence of reaction products as coronas around reactant grains together with diffusion-controlled zoning profiles in reactant grains are particularly indicative of disequilibrium on the scale of a thin section (cf. Korzhinskii, 1959; Thompson, 1959; Loomis, 1976).

It is notable that, in general, disequilibrium and partial equilibrium have only been recognized in rocks which preserve textures of incomplete reaction. If deformation affects a rock after reactions have occurred, the textural criteria for recognizing a disequilibrium assemblage are likely to be destroyed, and the origin of diffusion-controlled zoning profiles in minerals such as garnet may become uncertain. Under such circumstances it may be impossible to recognize disequilibrium between minerals in a thin section. However, deformation has a catalytic effect on reaction kinetics (Yund & Tullis, 1980; Brodie & Rutter, 1985), and it is tempting to assume that complete equilibrium is generally achieved during high-strain penetrative deformation (see Ridley & Dixon, 1984). One of the purposes of this paper is to show that path dependency, i.e. non-equilibrium effects, may be important in the determination of mineralogical and chemical behaviour and yet may not be discernible in petrographic analysis. In such cases the failure to recognize disequilibrium in deformed rocks may result in erroneous P–T estimates when thermobarometric techniques are applied. Using an orthogneiss from the Sesia Zone, Western Alps, Italy as an example of both equilibrium and disequilibrium processes we wish to demonstrate the possible complex relationships between reaction history, deformation history and the mineralogical evolution of deformed rocks.

We use the term 'mineral association' in this paper to describe a group of minerals that occur in close proximity within small volumes of a sample (see Tracy & McLellan, 1985). This term does not imply that the minerals were necessarily in equilibrium—which is suggested by the more familiar term 'mineral assemblage'. In our discussion of disequilibrium textures, we are not referring to the commonly observed phenomenon of mineral zoning interpreted as continuous reaction growth zoning.

Sesia Zone orthogneiss

The Sesia Zone is the most internal (southeastern) tectonic unit of the Western Alps and consists of a polymetamorphic crystalline basement with a range of quartzo-feldspathic, metacarbonaceous, pelitic, basic, and ultrabasic lithologies. Following pre-Alpine granulite to amphibolite facies metamorphism, this basement was metamorphosed in the eclogite facies ($P > 14$–16 kb, $T = 500$–560 °C) during early Alpine underthrusting and subduction (Compagnoni, 1977; Compagnoni *et al.*, 1977; Desmons & Ghent, 1977; Koons, 1982, 1986; Rubie, 1984*a*). A record of this high pressure metamorphism is well preserved in the various lithologies.

A large part of the central Sesia Zone (> 100 km^2) consists of foliated orthogneiss which varies in composition from quartz diorite to granodiorite and contains quartz + Na-pyroxene + garnet + phengite + paragonite + zoisite + sphene + minor sulphides (Fig. 1). Relatively rare enclaves or pods of metaquartz diorite, typically 100 m across, which have escaped penetrative deformation and in which the original igneous textures are well preserved, occur within this orthogneiss, notably on the east face of Monte Mucrone (Compagnoni & Maffeo, 1973; Rubie, 1983). The metaquartz diorite consists of quartz + jadeite + two muscovites + biotite + garnet + potassium feldspar + zoisite + sphene ± allanite. Although mineralogically quite different, the metaquartz diorite and the orthogneiss were evidently both derived from similar protoliths which originated as intrusive rocks of late Hercynian age (Oberhaensli *et al.*, 1982, 1985). A sequence of steps in the high-pressure evolution of the orthogneiss can be reconstructed if it is assumed that such a time sequence may be related to the spatial sequence observed in outcrop (see Ridley & Dixon, 1984, p. 122). The metaquartz diorite represents an early stage in the development of orthogneiss, and textures and mineral chemistry indicate a state of disequilibrium during

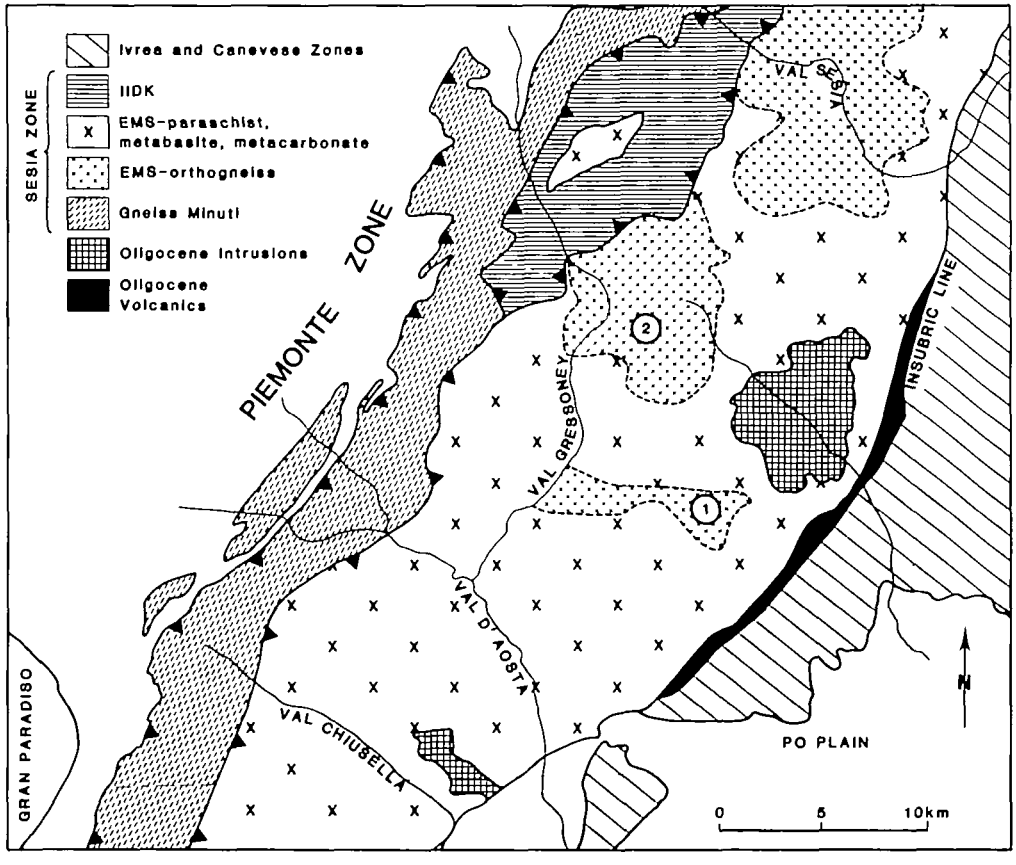

FIG. 1. Geological map of the central Sesia Zone showing the three main tectonic units: Seconda Zona diorito kinzigitica (IIDK), Eclogitic Micaschist Complex (EMS), and Gneiss Minuti (Campagnoni *et al.*, 1977; Rubie, 1984*a*). The EMS has been divided into regions consisting predominantly of orthogneiss and regions consisting predominantly of paraschist with metabasite, metacarbonate, orthogneiss, and ultramafics. Lenses of undeformed metaquartz diorite occur within the orthogneiss at Monte Mucrone (1) and Colle della Vecchia (2). (Modified from Compagnoni *et al.*, 1977.)

metamorphism. Subsequent deformation produced the orthogneiss via an intermediate 'transition orthogneiss' stage. This transition from metaquartz diorite to orthogneiss provides an excellent opportunity to study the effect of deformation on disequilibrium mineral associations and on the paragenesis of mineral associations, as well as the effect of metamorphism on deformation as discussed by Rubie (1983). Subsequent to high-pressure metamorphism, during uplift, rocks of the Sesia Zone including the orthogneiss were variably overprinted by first blueschist and then greenschist metamorphism. Details of this later evolutionary stage have been described by Compagnoni & Maffeo (1973) and Oberhaensli *et al.* (1985). Here we examine the mineralogy, microstructural evolution and possible reaction histories of metaquartz diorite, transition orthogneiss, and orthogneiss during high pressure metamorphism, in order to explain how mineralogical differences between rock types of similar composition, which have had identical pressure–temperature–time histories, can arise as a result of different deformation histories.

Chemical analyses of metaquartz diorite, transition orthogneiss and orthogneiss show some variability (Table 1). This may result from: (a) localized heterogeneities such as banding on the scale of a hand specimen in deformed rocks; and (b) larger scale compositional variation within the original intrusion. An additional alternative is that deformation was accompanied by fluid infiltration as discussed below (see also Oberhaensli *et al.*, 1985), and that infiltration was responsible for chemical changes. However, the textural evidence discussed below suggests that the variations in whole rock chemistry do not affect the conclusions presented in this paper.

TABLE 1

Representative whole rock chemical analyses of metaquartz diorite, transition orthogneiss and orthogneiss

	Metaquartz diorite			*Transition orthogneiss*					*Orthogneiss*		
	R81/186	*R81/189*	*13/3*	*R82/5*	*R81/185*	*13/1X*	*13/1Y*	*13/7*	*R82/9*	*R81/191BI*	*R81/191BII*
SiO_2	67·09	68·91	67·42	71·17	68·10	69·81	68·63	68·13	63·66	67·56	68·50
TiO_2	0·49	0·40	0·51	0·37	0·48	0·44	0·44	0·44	0·70	0·51	0·51
Al_2O_3	16·49	15·73	16·41	15·14	15·97	15·07	15·57	15·93	17·88	15·56	15·26
Fe_2O_3	0·13	0·27	0·19	0·46	0·95	0·87	1·01	0·75	0·96	1·16	0·72
FeO	3·55	2·80	3·40	2·35	2·90	2·45	2·40	2·75	3·65	3·15	3·45
MnO	0·05	0·04	0·05	0·04	0·04	0·05	0·05	0·05	0·06	0·07	0·07
MgO	1·03	0·75	1·01	0·72	0·93	0·86	0·87	0·83	1·51	1·53	1·44
CaO	3·68	3·10	4·02	3·34	3·73	2·72	3·08	3·21	4·54	4·38	4·16
Na_2O	3·55	3·45	3·19	3·43	3·55	2·99	3·43	3·28	3·67	3·64	3·37
K_2O	2·73	3·21	2·60	1·65	1·85	3·30	3·27	2·75	1·46	0·98	1·00
P_2O_5	0·15	0·14	0·18	0·08	0·14	0·13	0·13	0·13	0·22	0·15	0·15
H_2O^+	0·84	0·83	0·85	1·00	1·18	1·19	1·29	1·47	1·53	1·16	1·51
CO_2	0·12	0·08	0·12	0·14	0·13	0·06	0·10	0·18	0·02	0·04	0·02
Total	99·90	99·71	99·95	99·89	99·95	99·94	100·27	99·90	99·86	99·89	100·16

METAQUARTZ DIORITE

Petrography and mineralogy

The original quartz diorite is thought to have consisted of quartz (30–40 per cent) + plagioclase ($<An_{20}$?, 40–50 per cent) + biotite ± potassium feldspar ± allanite. Within minor enclaves which lack penetrative deformation, the original igneous textures have survived the high-pressure metamorphism. Three domains in these metaquartz diorite enclaves are distinguished on the basis of mineralogy and texture (Figs. 2a, b and 3): Domain

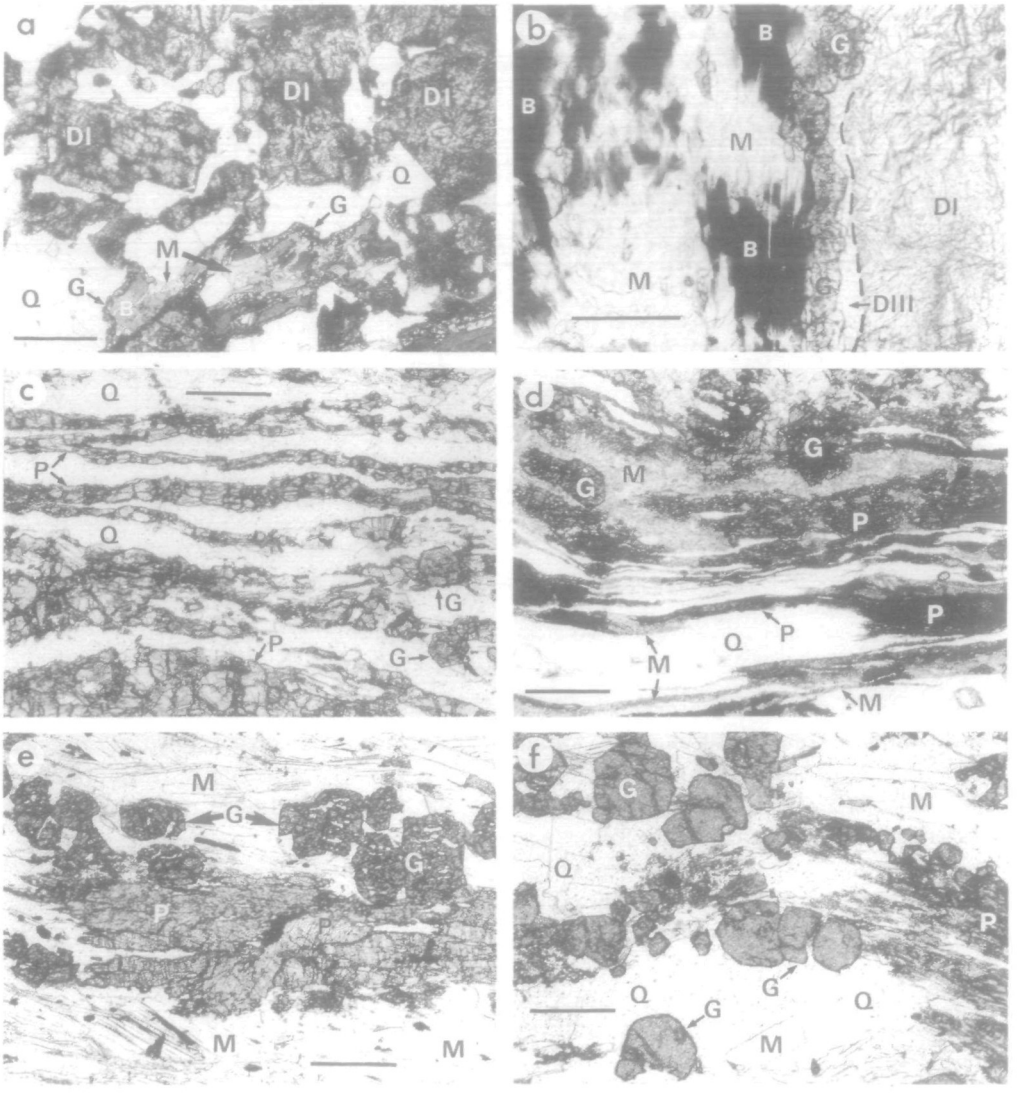

FIG. 2. Photomicrographs of metaquartz diorite (a, b), transition orthogneiss (c, d), and orthogneiss (e, f). Plane polarized light. (a) Metaquartz diorite showing Domain I aggregates of fine-grained jadeite + quartz + zoisite pseudomorphing plagioclase (DI), medium-grained quartz (Q), and an example of Domain II at bottom centre. The latter consists of flakes of biotite (B) partially replaced by fine-grained muscovite 1 (M) and rimmed by a narrow garnet corona (G). (See also Compagnoni & Maffeo, 1973, figs. 4–8 and Rubie, 1983, fig. 6) Scale bar = 0·5 mm. (b) Domains I, II and III in metaquartz diorite. Domain II occupies the left hand half of the photomicrograph and consists of relict biotite (B), muscovite 1 (M), and a garnet corona (G) immediately right of centre. Domain I (DI), situated to the right, is separated from Domain II by Domain III (DIII) consisting of muscovite 2 + quartz. Scale bar = 0·5 mm. (c) Transition orthogneiss—superplastically deformed pyroxene-rich layers (P) separated by layers of medium-grained quartz (Q). The pyroxene has a grain size of ~ 0·2 mm. Two euhedral garnets (G) are located on the far right. (See also Rubie, 1983, fig. 7a.) Scale bar = 0·5 mm. (d) Transition orthogneiss—superplastically deformed pyroxene-rich layers (P) partially replaced by fine-grained aggregates of phengitic muscovite (M) possibly as a consequence of fluid infiltration during and/or after deformation. Medium-grained quartz lenses (Q) and euhedral to subhedral garnets (G) are also present. Scale bar = 0·5 mm. (e) Typical orthogneiss showing an aggregate of omphacitic pyroxene (P), garnets (G) with quartz inclusions, and medium-grained aggregates of white mica (M) consisting of both phengite and paragonite. Scale bar = 0.5 mm. (f) Orthogneiss—garnets (G), showing textural evidence for partial resorption, in a matrix of medium-grained quartz (Q) with scattered flakes of phengite and paragonite (M). A pyroxene relic (P), strongly affected by greenschist overprinting, is situated on the right. Scale bar = 0·5 mm.

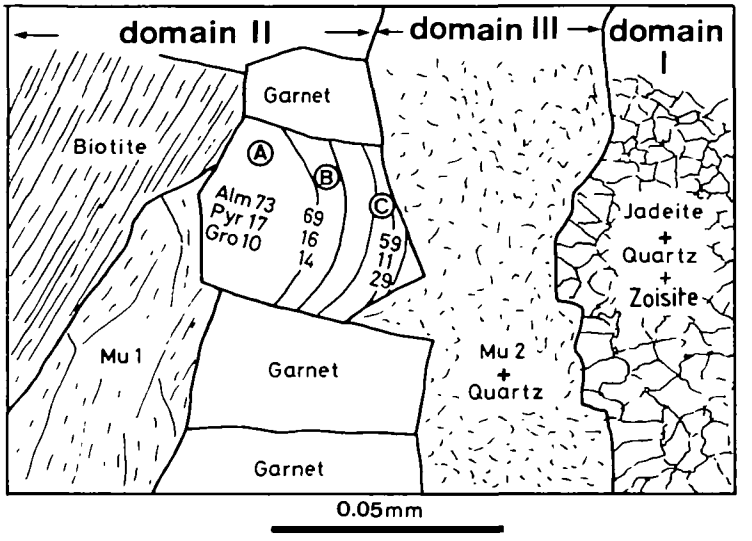

FIG. 3. Diagrammatic sketch showing textural relationships between Domains I, II, and III in metaquartz diorite (cf. Fig. 2b). The garnets of Domain II are typically <0·50 μm diameter, and a typical compositional zonation pattern in one of the garnets is shown by contours of percentage almandine (Alm), pyrope (Pyr) and grossular (Gro) contents. Analyses of points at A, B, and C are given in Table 4. (Mu1—muscovite 1, Mu2—muscovite 2.)

I—fine-grained jadeite + quartz + zoisite pseudomorphing plagioclase; Domain II—biotite + high-titanium phengite + garnet, Domain III—phengitic muscovite + quartz + sphene. The remainder of the rock consists primarily of quartz with occasional potassium feldspar and allanite (Fig. 2a, b). Large quartz grains show strongly undulose extinction and are mantled by strain-free recrystallized grains.

The following domain descriptions are in general representative of the textural relations found throughout the bulk of the rock (Fig. 3), although some divergence from the geometries described here does occur.

Domain I

Fine-grained (20–60 μm dia.), variably oriented, xenoblastic pyroxene constitutes 80 per cent or more of Domain I. Needles of zoisite (~15 μm long, ~1 μm dia.) and equally small needles and blebs of quartz are contained within the pyroxene aggregate (Compagnoni & Maffeo, 1973; Rubie, 1983, fig. 6b). The averaged structural formula of the pyroxene is

$$Na_{0\cdot92}Ca_{0\cdot05}Fe^{2+}_{0\cdot03}Mg_{0\cdot01}Al_{0\cdot97}Si_{2\cdot00}O_{6\cdot0}$$

and microprobe analyses often indicate minor excess alumina. Although the jadeite content of the pyroxenes is fairly constant ($X_{Jd} = 0{\cdot}85$–$0{\cdot}93$, $X_{Mg} = Mg/(Mg + Fe^{2+})$) shows considerable variation from 0 to 0·45 (Fig. 4, Table 2). The possibility that some zoisite component is included in these analyses (due to the small grain size) makes the estimates of jadeite content minimum ones, and may also explain the slight apparent Ca-Tschermaks component which is seldom present in high-pressure, low-temperature pyroxenes.

Domain II

Biotite which forms the core of Domain II is a coarse-grained (1–3 mm), dark red, high titanium variety with an averaged structural formula of

$$K_{0\cdot95}Fe^{2+}_{0\cdot90}Mg_{1\cdot30}Ti_{0\cdot29}Al_{1\cdot14}Si_{2\cdot90}O_{10}(OH)_2$$

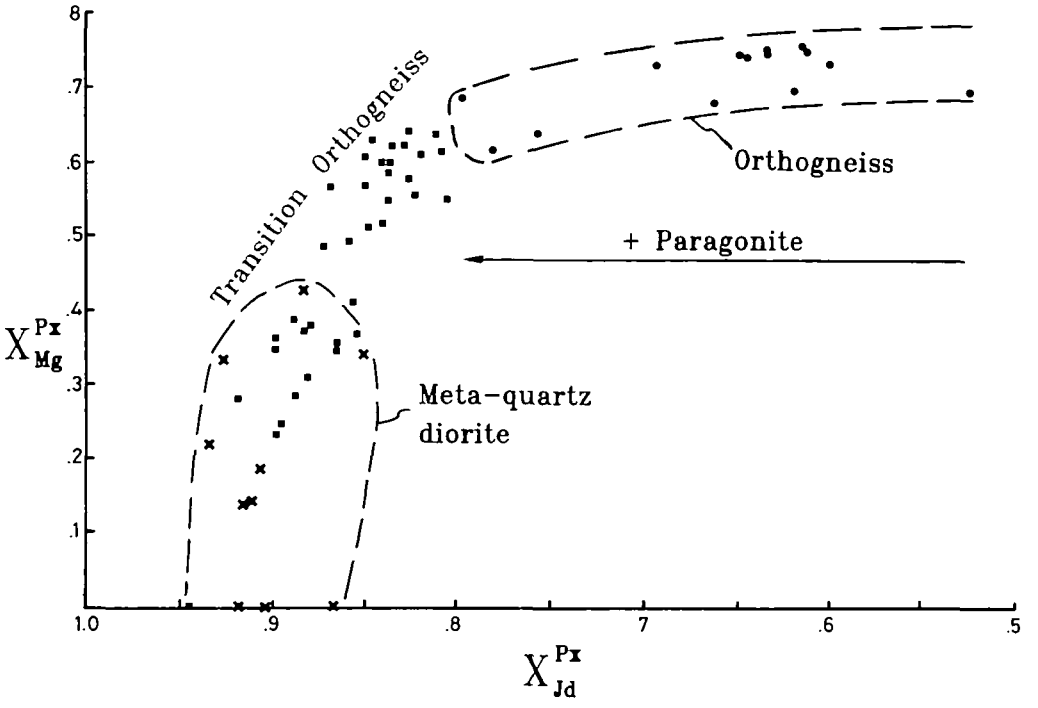

FIG. 4. Compositions of pyroxenes in metaquartz diorite (crosses), transition orthogneiss (squares) and orthogneiss (circles) plotted as X_{Mg} (= Mg/(Mg + Fe^{2+})) against jadeite content (X_{Jd} = jadeite/(jadeite + diopside + acmite)). Compositions have been calculated from analyses by normalizing the cations to a total of 6 oxygens and then by following method 1 of Essene & Fyfe (1967, p. 15) (see Table 2). As the acmite content is very low in all of these pyroxenes ($X_{Ac} < 0{\cdot}02$), their compositions lie close to the jadeite–diopside join (Table 2). Paragonite coexists with pyroxenes in the orthogneiss, but is absent in the metaquartz diorite and transition orthogneiss.

(Table 3). The biotite, which is clearly of magmatic origin, is apparently compositionally homogeneous throughout the rock, and no compositional zoning has been detected. Individual biotite flakes are partially or completely surrounded by leaves of muscovite and small euhedral garnets.

The muscovite of Domain II is a fine-grained (0·02–0·5 mm), high-titanium phengite referred to hereafter as 'muscovite 1'. The averaged structural formula of muscovite 1 is

$$K_{0\cdot85}Fe_{(tot)0\cdot13}Mg_{0\cdot36}Ti_{0\cdot14}Al_{1\cdot39}Al_{0\cdot61}Si_{3\cdot39}O_{10}(OH)_2$$

(Fig. 5, Table 3), and it exhibits no detectable compositional zoning. Muscovite grains are commonly interleaved with biotite and often completely surround individual biotite grains, while the other edge of the muscovite is adjacent to either the euhedral garnets or the Domain II/Domain III interface.

Garnets form a partial corona around the Domain II cores of biotite and muscovite 1. Individual garnets have very few inclusions, are idiomorphic with a diameter of 0·01–0·2 mm, and exhibit sharp growth surfaces adjacent to other phases. A typical zonation pattern is shown in Fig. 3. In the region of a garnet crystal adjacent to biotite or muscovite 1 the almandine content remains approximately constant at ~75 per cent from core to rim (Figs 3 and 6, Table 4). The zoning pattern in that portion of a garnet oriented towards domains I and III, and therefore away from biotite, varies from $\sim Alm_{0\cdot70}Gro_{0\cdot10}$ at the core to

TABLE 2

Representative electron microprobe analyses of pyroxenes

	Metaquartz diorite 18333			*Transition orthogneiss R81/185*			*Orthogneiss R81/191B*	
SiO_2	58·38	58·85	57·06	58·98	58·89	58·72	57·44	55·96
TiO_2	0·00	0·00	0·00	0·00	0·00	0·00	0·00	0·00
Al_2O_3	25·53	24·79	25·43	22·08	21·02	21·48	18·99	12·71
FeO	0·56	0·44	0·90	3·39	2·88	2·17	2·85	4·91
MgO	0·00	0·07	0·26	0·62	1·73	1·83	2·57	6·35
CaO	1·66	0·97	2·67	1·64	3·30	3·59	4·63	10·89
Na_2O	13·80	14·21	12·87	13·08	12·34	12·45	11·69	8·00
K_2O	0·00	0·04	0·03	0·00	0·00	0·00	0·00	0·00
Total	99·92	99·36	99·23	99·80	100·17	100·24	98·17	98·87
	Cations based on 6 oxygens							
Si	1·973	1·997	1·950	2·020	2·014	2·003	2·016	2·005
Ti	0·000	0·000	0·000	0·000	0·000	0·000	0·000	0·001
Al^{IV}	0·027	0·003	0·050	—	—	—	—	—
Al^{VI}	0·990	0·988	0·974	0·891	0·848	0·864	0·786	0·537
Fe^{2+}	0·016	0·012	0·026	0·097	0·082	0·062	0·085	0·165
Fe^{3+}	—	—	—	—	—	—	0·009	0·018
Mg	0·000	0·003	0·013	0·032	0·088	0·093	0·134	0·339
Ca	0·060	0·035	0·098	0·060	0·121	0·131	0·174	0·418
Na	0·904	0·935	0·853	0·869	0·818	0·824	0·795	0·555
K	0·000	0·002	0·001	0·000	0·000	0·000	0·000	0·000
Total	3·970	3·976	3·965	3·969	3·971	3·977	3·999	4·003
Jadeite	0·90	0·94	0·85	0·87	0·82	0·82	0·79	0·54
Acmite	0·00	0·00	0·00	0·00	0·00	0·00	0·01	0·02
Augite	0·06	0·04	0·10	0·06	0·12	0·13	0·17	0·42
X_{Mg}	0·00	0·20	0·33	0·25	0·52	0·60	0·64	0·67

$Fe^{3+} = Na - Al^{VI}$; $Fe^{2+} = Fe$ (total) $- Fe^{3+}$; Jadeite $= Na - Fe^{3+}$; Acmite $= Fe^{3+}$; Augite $= Ca$.

$\sim Alm_{0·60}\ Gro_{0·30}$ at the rim (Figs. 3 and 6, Table 4). Zoisite is occasionally found within the garnet coronas.

Domain III

Fine-grained muscovite + quartz with minor zoisite and sphene form the mineral association of Domain III which spatially separates Domain I from Domain II (Figs. 2 and 3). The muscovite of Domain III is hereafter referred to as muscovite 2. Compared with muscovite 1, it has distinctly lower values of TiO_2, FeO, and MgO, variable amounts SiO_2, and a higher value of Al_2O_3 (Fig. 5, Table 3). The averaged structural formula is

$$\sim Na_{0·01}K_{0·86}Fe_{(tot)0·10}Mg_{0·30}Ti_{0·01}Al_{1·62}Al_{0·62}Si_{3·38}O_{10}(OH)_2.$$

The contacts of Domain III with the other domains are sharp, and occur over a distance of 10 μm or less.

The amount of potassium feldspar originally present in these rocks is difficult to estimate due to sporadic overprinting by muscovite 2 (see also Hy, 1984).

TRANSITION ORTHOGNEISS

The transition orthogneiss is a fine- to medium-grained rock, with a strong planar fabric, which is distinguished from orthogneiss on the basis of microstructure and mineralogy. It

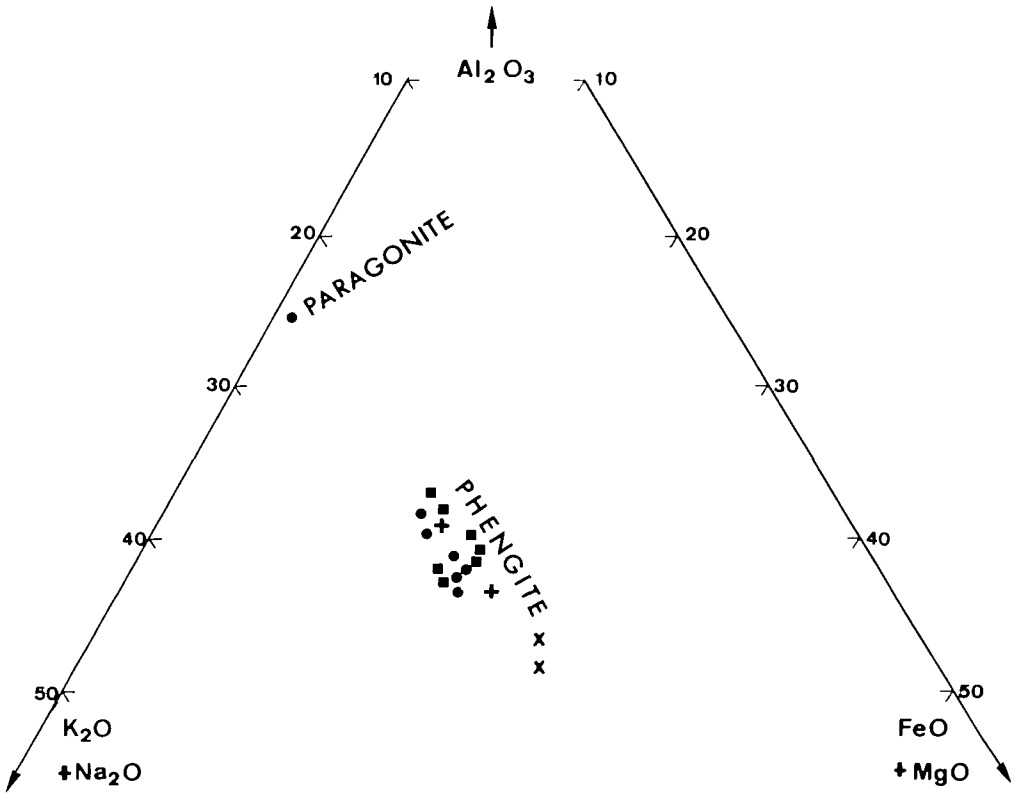

FIG. 5. Compositions of phengite and paragonite in metaquartz diorite (crosses), transition orthogneiss (squares) and orthogneiss (circles), showing the variation in the tschermak content of phengite. Metaquartz diorite micas from Domains I and II are shown: × —muscovite 1, + —muscovite 2. Although transition orthogneiss and orthogneiss phengites show some compositional variation on this diagram, this variation is much more restricted within a single thin section.

was formed by high-strain deformation of metaquartz diorite, and occurs in zones which separate pods of metaquartz diorite from orthogneiss and also in narrow (< 20 cm wide) ductile shear zones within metaquartz diorite. Veins of garnet ($\sim Alm_{0\cdot35}Gro_{0\cdot65}$) + zoisite ± quartz (1–2 cm wide) are located along many of these shear zones.

Petrography and mineralogy

The transition orthogneiss is characterized by thin (0·2–0·5 mm wide) semi-continuous layers of Na-pyroxene + quartz ± zoisite which define a strong planar fabric. These resulted from intense deformation of plagioclase pseudomorphs (Domain I) of the metaquartz diorite (Fig. 2c, d). The pyroxenes in these layers are no longer fine-grained but generally occupy the full width of a layer. In the layers contained within zones of transition orthogneiss situated between metaquartz diorite and orthogneiss, pyroxene has uniform extinction, quartz generally forms a small number of large inclusions, and zoisite is often absent from these layers (Fig. 2c). However, in the narrow shear zones, pyroxene often exhibits strongly undulose extinction and contains numerous submicroscopic inclusions of quartz and zoisite. These differences may indicate contrasting annealing histories. Average compositions of

TABLE 3

Representative electron microprobe analyses of micas

	Metaquartz diorite 18333			*Transition orthogneiss R81/185 R82/4*		*Orthogneiss R82/9R81/191B*		*R82/9R81/191B*	
	Bio	*Mu 1*	*Mu 2*	*Muscovite*		*Muscovite*		*Paragonite*	
SiO_2	39·54	51·59	51 23	49·98	48·67	48·97	49·09	46·10	46·44
TiO_2	5·42	2·81	0·40	0·56	0·56	0·41	0·33	0·11	0·05
Al_2O_3	12·99	26·27	28·63	31·52	28·68	31·34	29·36	38·22	38·35
Cr_2O_3	0·00	0·00	0·00	0·00	0·00	0·00	0·00	0·00	0·03
FeO	15·12	2·19	1·83	1·53	2·17	1·26	1 83	0·17	0·31
MnO	0·04	0·00	0·00	0·00	0·00	0·00	0·00	0·00	0·00
MgO	11·80	3·66	3·15	2·05	2·20	2·26	2·65	0·11	0·11
CaO	0·00	0·00	0·00	0·00	0·00	0·00	0·03	0·26	0·23
Na_2O	0·03	0·07	0·11	0·72	0·50	1·09	0·96	7·08	6·34
K_2O	10·02	9·59	10·30	9·72	10·46	9·55	9·27	0·76	0·89
Total	94·96	96·20	95·66	96·08	93·24	94·88	93·51	92·81	92·75
	Cations based on 11 oxygens								
Si	2·961	3 391	3·383	3·277	3·322	3·254	3·314	3·020	2·943
Ti	0·305	0·139	0·020	0·028	0·029	0·020	0·017	0·005	0·002
Al^{IV}	1·039	0·609	0·617	0·723	0·678	0·746	0·686	0 980	1·057
Al^{VI}	0·108	1·427	1·611	1·713	1·630	1·709	1·651	1·973	1·809
Cr	0·000	0·000	0·000	0·000	0·000	0·000	0·000	0·000	0·023
Fe	0·947	0·121	0·101	0·084	0·124	0·070	0·103	0·009	0·016
Mn	0·002	0·000	0·000	0·000	0·000	0·000	0·000	0·000	0·000
Mg	1 317	0·359	0·310	0·200	0·224	0·224	0·267	0·010	0·010
Ca	0·000	0·000	0·000	0·000	0·000	0·000	0·002	0·018	0·016
Na	0·005	0·009	0·015	0·092	0·066	0·140	0·126	0·900	0·779
K	0·958	0·804	0·867	0·813	0·911	0·810	0·798	0·064	0·072
Total	7·642	6·858	6·924	6 930	6·983	6·973	6·963	6·980	6 727

Mu 1 = muscovite 1, Mu 2 = muscovite 2

pyroxenes are slightly less jadeitic and more magnesian than pyroxenes of the metaquartz diorite (Fig. 4, Table 2). Variation in composition is notable. X_{Jd} can range from 0·80 to 0·85 and X_{Mg} from 0 to 0·65 within a single thin section (Fig. 4).

Discontinuous layers and lenses of medium-grained quartz which often show a well developed foam texture, separate the pyroxene-rich layers (see van Roermund *et al.*, 1979).

Euhedral garnets up to 0·75 mm dia. (an order of magnitude larger than in the metaquartz diorite) are common. In some samples the garnets are almost homogeneous, whereas in others the crystals are zoned, ranging from $Alm_{0·46}Gro_{0·52}$ in the cores to $Alm_{0·57}Gro_{0\ 38}$ along the rims (Table 4, Fig. 6). However, in shear zones with associated veins of grossular-rich garnet + zoisite, cores of $Alm_{0·60}Gro_{0·38}$ are surrounded by rims of $Alm_{0·42}Gro_{0·56}$. No garnets with the assymetric zoning patterns characteristic of the metaquartz diorite have been found. Minute inclusions of sphene or rutile are common in the garnets.

In the transition orthogneiss, phengite forms flakes, up to 0·7 mm long, which are frequently concentrated in layers and weakly aligned parallel to the planar fabric. In contrast, phengites in shear zones in metaquartz diorite are often very fine-grained and are sometimes associated with the pyroxene-rich layers (Fig. 2d). The composition of the phengite is similar to muscovite 2 of the metaquartz diorite (Fig. 5, Table 3). Biotite is absent in the transition orthogneiss, but occasionally occurs as relicts in the narrow shear zones.

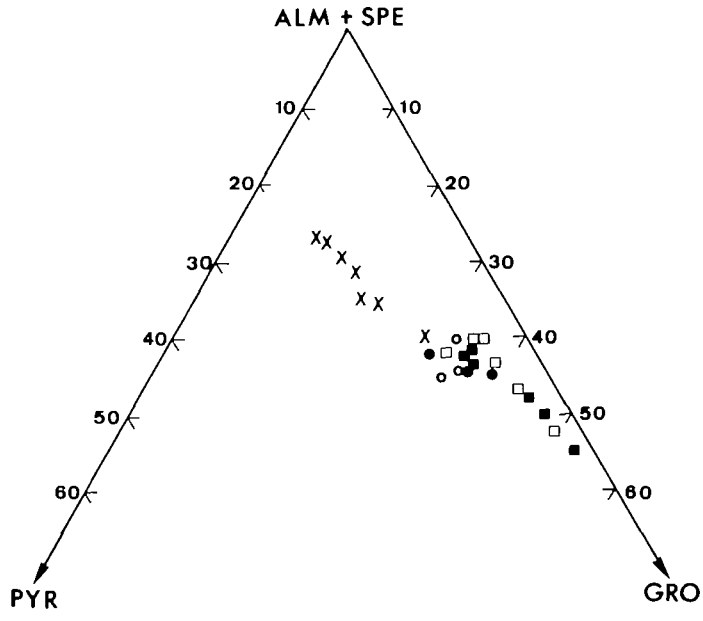

FIG. 6. Compositions of garnets in metaquartz diorite (crosses), transition orthogneiss (squares) and orthogneiss (circles) plotted in terms of almandine + spessartine (Alm + Spe), pyrope (Pyr) and grossular (Gro) components. Closed symbols are core compositions and open symbols are rim compositions. The metaquartz diorite analyses show the variation from rim to rim across a typical single 50 μm diameter crystal such as the one shown in Fig. 3.

Zoisite forms slender prisms, up to 0·7 mm long, and is often associated with micaceous layers. In the narrow shear zones, zoisite is mainly present (together with quartz) as very fine-grained inclusions in the pyroxene-rich layers. Potassium feldspar has not been found in these deformed rocks.

ORTHOGNEISS

The orthogneiss is a medium-grained rock, with a well developed planar fabric defined by the preferred orientation of micas and elongate pyroxenes (Fig. 2e, f), which outcrops over a large area in the central Sesia Zone (Fig. 1). It evolved from the transition orthogneiss by further deformation, and consists of quartz + Na-pyroxene + garnet + phengite + paragonite + zoisite + sphene ± rutile + minor sulphides (see also Oberhaensli *et al.*, 1985). Zoning patterns in pyroxenes and the general absence of amphibole as part of the high pressure assemblage distinguish the orthogneiss from other common Sesia Zone lithologies.

Petrography and mineralogy

The sodic pyroxenes of the orthogneiss are commonly medium to large (2–4 mm long) lath-like crystals with irregular grain boundaries (Fig. 2e). In some samples there is clear evidence that these individual pyroxenes were formed by disruption of the pyroxene layers which characterize the transition orthogneiss. These pyroxenes exhibit a greater compositional variation than do sodic pyroxenes from other common rock types in the Sesia Zone (Koons, 1982), and range from $X_{Jd} > 0{\cdot}80$ to $X_{Jd} = 0{\cdot}50$ (Fig. 4, Table 2). X_{Mg} ranges from 0·60–0·75, although within a single thin section the range is generally much more limited. The

TABLE 4

Representative electron microprobe analyses of garnets

	Metaquartz diorite			*Transition orthogneiss*		*Orthogneiss*			
	18333			*R81/185*	*R82/3*	*R81/191B*			
	(A)	*(B)*	*(C)*	*Core*	*Rim*	*Core*	*Rim*	*Core*	*Rim*
SiO_2	38·23	38·41	38·66	37·37	37·88	37·90	37·55	38·01	38·21
TiO_2	0·09	0·12	0·08	0·05	0·00	0·00	0·05	0·10	0·00
Al_2O_3	21·21	21·37	21·14	20·95	21·39	21·22	21·27	21·57	21·49
Cr_2O_3	0·00	0·05	0·05	0·00	0·00	0·00	0·00	0·00	0·00
FeO	32·04	31·18	27·07	26·19	25·96	20·50	25·39	25·61	24·88
MnO	0·71	0·68	0·43	0·33	0·40	0·39	0·67	0·40	0·39
MgO	4·32	3·94	2·85	1·71	2·60	0·51	1·24	3·06	2·81
CaO	3·35	4·78	10·15	12·06	11·21	18·72	13·50	10·44	11·87
Na_2O	0·03	0·07	0·03	0·00	0·00	0·00	0·06	0·03	0·00
K_2O	0·03	0·03	0·04	0·00	0·02	0·00	0·01	0·02	0·01
Total	100·02	100·63	100·50	98·67	99·46	99·23	99·75	99·22	99·67
	Cations based on 12 oxygens								
Si	3·027	3·021	3·031	2·999	3·000	3·000	2·985	3·004	3·007
Ti	0·006	0·007	0·005	0·003	0·000	0·000	0·003	0·006	0·000
Al	1·979	1·981	1·953	1·982	1·996	1·980	1·993	2·009	1·993
Cr	0·000	0·003	0·003	0·000	0·000	0·000	0·000	0·000	0·000
Fe	2·121	2·051	1·775	1·758	1·719	1·357	1·688	1·693	1·638
Mn	0·047	0·045	0·029	0·023	0·027	0·026	0·045	0·027	0·026
Mg	0·510	0·462	0·333	0·205	0·307	0·060	0·147	0·360	0·330
Ca	0·284	0·403	0·853	1·037	0·952	1·588	1·150	0·884	1·001
Na	0·005	0·010	0·005	0·000	0·000	0·000	0·009	0·005	0·000
K	0·003	0·003	0·004	0·000	0·002	0·000	0·001	0·002	0·001
Total	7·982	7·986	7·990	8·007	8·003	8·010	8·021	7·989	7·997
Alm	0·72	0·69	0·59	0·58	0·57	0·45	0·56	0·57	0·55
Spe	0·02	0·01	0·01	0·01	0·01	0·01	0·01	0·01	0·01
Pyr	0·17	0·16	0·11	0·07	0·10	0·02	0·05	0·12	0·11
Gro	0·09	0·14	0·29	0·34	0·32	0·52	0·38	0·30	0·33

Analyses A, B and C refer to Fig. 3.

pyroxenes show a compositional amalgam rather than a clear zonation pattern, with domains of jadeitic pyroxene adjacent to and occasionally surrounded by regions of more omphacitic pyroxene. Although some jadeitic domains appear, on the basis of being surrounded by omphacite, to predate the omphacitic domains, there are no clear compositional relationships as found in other Sesia Zone rocks of quartzo–feldspathic composition (Koons, 1982, 1986). The pyroxenes in the orthogneiss often contain intergrowths or inclusions of paragonite and garnet.

Garnets are usually small (<0·8 mm diam.) and exhibit both regular and irregular grain boundaries suggesting that partial resorption has occurred (Fig. 2f). The garnets are compositionally similar to those of the transition orthogneiss and show irregular zonation patterns, with relatively small compositional variations (Fig. 6, Table 4). The average grossular content of 34 per cent is unusually high for quartz-bearing rocks from the Sesia Zone (Koons, 1982).

A large modal percentage of phengite, and particularly the large amount of paragonite, distinguish the orthogneiss from the metaquartz diorite and transition orthogneiss in which paragonite is absent. Both micas occur as large sheets (up to 2 mm long) which define the main foliation (Fig. 2e, f). Paragonite also commonly occurs as fine-grained intergrowths

with pyroxene and garnet. Little compositional variation was found in either phengite or paragonite, with the latter being very similar in composition to paragonite found in other Sesia Zone assemblages. The composition of phengite is very similar to muscovite 2 of Domain III in the metaquartz diorite (Fig. 5, Table 3), and is more aluminous (less phengitic) than phengites from other rock types of the Sesia Zone (Koons, 1982).

Zoisite occurs as prisms up to 0·6 mm long, and in some samples is only present as an accessory mineral. Subhedral grains of sphene, often with cores of rutile, are associated with mica-rich layers.

Although amphibole is generally absent from the high-pressure assemblage, Compagnoni & Maffeo (1973, p. 368) reported rare glaucophane in some xenolithic inclusions.

REACTION BEHAVIOUR IN THE METAQUARTZ DIORITE

The distinctive petrochemical evolution of the metaquartz diorite as discussed above is not adequately described by equilibrium thermodynamic theory and non-equilibrium theory must be invoked to effectively describe the observed behaviour. The irreversible thermodynamics of the interrelationships of chemical reaction and diffusion have been successfully described for systems close to equilibrium through a phenomenological treatment by, among others, de Groot & Mazur (1962), Katchalsky & Curran (1965), and Prigogine (1967). More recent work by Fisher (1973, 1977), Weare *et al.* (1976), and Foster (1977, 1981) has illustrated the value of the phenomenological approach in the description of geological processes. The great strength of the phenomenological treatment in the description of diffusion related processes lies in the effective bridging of the gap between chemical and physical driving forces by relating the affinities of reaction ($A = -\Sigma n_1 \mu_i$ (n_1 and μ_i are, respectively, the number of moles and the chemical potential of component i)) to spatial derivatives ($= \nabla \mu_i$) for near-equilibrium systems which are dominated by continuous processes. The approach is particularly useful in the description of metasomatic aureole growth in which the geometry is relatively simple (see Joesten, 1977). The following discussion deals with a qualitative treatment of reaction and diffusion as they apply to the evolution of the Sesia Zone orthogneiss. Numerical and analytical solutions of these equations are produced elsewhere (Koons, in prep.)

Reaction rates at any position within the reaction volume are related to the chemical potentials of the system components, at that position, through the phenomenological equations:

$$J_R = L_R A$$
$$J_D = L_D \nabla \mu_i \qquad (1)$$

where J_R is the reaction rate, J_D is the diffusion rate, and L_R and L_D are the phenomenological coefficients (from Prigogine, 1967).

The characteristic domain chemistry of the metaquartz diorite mineral associations suggests that the evolution of the metaquartz diorite was diffusion controlled (see Fisher, 1977 for a discussion of diffusion versus reaction controlled textures). Because diffusion appears to be the rate-limiting process, an evolution of the reaction rates and textural evolution in three dimensions is therefore dependent primarily upon evaluation of the chemical potentials of each component at any arbitrary position within the reaction volume: i.e. spatial mapping of reaction driving forces is crucially dependent upon spatial mapping of the chemical potentials of the system components. Once the chemical potentials as a function

of space are determined, the solution of the cross matrices relating affinities to the potentials (Eq. 1) will follow. In an isotropic medium the determination of the spatial values of μ_i may be accomplished through evaluation of the diffusion equation:

$$\partial\mu_i/\partial t = D_i\nabla^2\mu_i + P_i \tag{2}$$

where D_i is the diffusion coefficient of component i and P_i is the source/sink term for component i.

In diffusion-controlled processes, the timing of reactions and reaction rates are important in the determination of the source or sink term. Although the source/sink term is not a temporal function, the region in P–T–t volume occupied by a particular reaction defines the availability of the reactants. Assuming incompressibility and spatial independence of the diffusion coefficient, D, transient or steady state solutions of the diffusion equations may be obtained for any component, i. The steady state equations may be further defined on the basis of the presence or absence of a source/sink term within the region under consideration:

$$\nabla^2\mu_i = 0 \text{ (Laplace solution)} \tag{3}$$

$$\nabla^2\mu_i = P_i/D_i \text{ (Poisson solution).} \tag{4}$$

Several points about the following discussion of the metaquartz diorite must be emphasized: (1) In order to simplify the description of mass transfer, diffusing components are referred to as oxides. This does not imply that the components are believed to migrate as discrete oxide phases, but reflects the lack of information available on the state of complexing of migrating components (see also Fisher, 1973; Koons, 1981). (2) Due to large and poorly-quantified volume changes as well as the difficulty in identifying the mobile complexes, it is not possible to determine or reproduce the precise reactions responsible for the observed mineral chemistries. Given these constraints we have attempted to produce approximate descriptive reactions which fit the observed textures. Unless specified, reactions as written do not imply reversible equilibria, but rather describe irreversible transitions. (3) Local variations from the descriptions listed here may be expected to occur due to original mineralogical heterogeneity. What follows is therefore a description of the general reaction and diffusion behaviour during evolution of the various domains.

Either during or after the rapid pressure increase associated with the early Alpine collisional event (Rubie, 1983; Oberhaensli *et al.*, 1985), transition of igneous plagioclase in Domain I to higher pressure assemblages commenced by reactions of the type:

$$\text{plagioclase} \rightarrow \text{jadeite} + CaO + Al_2O_3 + SiO_2. \qquad \text{(Reaction 1)}$$

There is no mineralogic evidence to indicate either that the breakdown of feldspar was a continuous process of albitisation with increasing pressure prior to the crossing of the

$$\text{albite} \rightarrow \text{jadeite} + SiO_2 \qquad \text{(Reaction 2)}$$

equilibrium, or that the plagioclase remained metastably at the original igneous composition until reaction 2 was significantly overstepped and rapid reaction occurred. (See Rubie, 1983, for a discussion of the kinetics involved in this reaction.) In either case, the breakdown of plagioclase served as a CaO and Al_2O_3 source as well as producing the fine-grained interlocking texture of jadeite, zoisite and quartz diagnostic of Domain I.

The presence or absence of zoisite in Domains I and III as a CaO–Al_2O_3 sink is thought to be controlled by the availability of H_2O through the reaction:

$$CaAl_2Si_2O_{8(\text{plagioclase})} + H_2O \rightarrow \text{zoisite} + SiO_2 + Al_2O_3. \qquad \text{(Reaction 3)}$$

Associated with the rapid pressure increase was the initiation of a biotite breakdown reaction in Domain II. One of the distinctive mineralogical features of the metaquartz diorite is the lack of complete biotite reaction and the consequent preservation of biotite cores within coronas of muscovite 1 and garnet. This type of texture, generally attributed to diffusion-controlled processes (Fisher, 1977), together with the observed phase chemistries (i.e. high-titanium muscovites and some grossular component in even the cores of garnets) suggest that diffusion of CaO and Al_2O_3 from Domain I influenced the breakdown of biotite in a transition similar to:

$$\text{biotite} + Al_2O_3 + CaO \rightarrow \text{muscovite 1} + \text{garnet}. \qquad \text{(Reaction 4)}$$

The rate-determining step in this transition is the transport of Al_2O_3 and CaO from Domain I to the loci of reaction in Domain II. Continuous reactions among the AFM phases of Domain II may have further defined the compositions of these phases through the relations:

$$\text{biotite} \rightarrow \text{muscovite 1} + \text{garnet} - Al_2Mg_{-1}Si_{-1}(\text{biotite, muscovite}). \qquad \text{(Reaction 5)}$$

The cause of the lack of complete reaction may be twofold: (1) The muscovite 1 + garnet coronas decrease the diffusion coefficients, D_{CaO} and $D_{Al_2O_3}$ sufficiently to inhibit transport of the diffusing species to the reaction sites. In this case, D_i is strongly spatially dependent and the solutions of the transport equations become more complex than presented above. (2) The production of Al_2O_3 and CaO ceases in Domain I due to completion of the plagioclase breakdown reaction. The plagioclase breakdown reaction may be thought of as a $\mu_{Al_2O_3}$ and μ_{CaO} spike which migrates as a pulse from Domain I in a manner described by the transient diffusion equation (Eq. 2). The breakdown of biotite is a response to this transient pulse and ceases as the pulse decays with time. The presence of zoisite sinks due to the availability of H_2O within Domains I and II serves to dampen the μ_{CaO} and $\mu_{Al_2O_3}$ pulse. In these rocks without penetrative deformation, the extent of the biotite breakdown is therefore a function of the original plagioclase to biotite ratio as well as of the amount of H_2O available within the reaction volume.

As Domain II evolved with the formation of garnet + muscovite 1 rims around the biotites contemporaneous with migration of CaO from Domain I, the μ_{CaO}: $\mu_{(MgO+FeO)}$ ratios on the external (Domain I-facing) edges of these rims became higher than the ratio on the internal (biotite-facing) edges. Hence, during growth, garnet compositions were buffered under differing μ_{CaO}: $\mu_{(MgO+FeO)}$ conditions simultaneously at different positions relative to the domain geometries. These spatially related chemical potential differences yielded the distinctive assymetric zonation pattern in the garnets (Fig. 3) of higher grossular component in the Domain I-facing garnet rims.

The muscovite 1–2 transition in Domain III lies between Domains I and II and defines the response of the high-titanium muscovite 1 to increasing levels of $\mu_{Al_2O_3}$ and μ_{CaO} associated with Domain I. This transition may be described by the reaction

$$\text{muscovite 1} + CaO + Al_2O_3 \rightarrow \text{muscovite 2} + \text{sphene} \qquad \text{(Reaction 6)}$$

which accounts for the fine-grained sphene associated with the low-titanium muscovite 2. The composition of muscovite 2 is similar to the phengites which are found throughout high-pressure terranes. The role of potassium feldspar in these reactions, either as an individual phase or as a perthite component of the original feldspar is not clear. In the presence of H_2O, muscovite 2 may form directly from potassium feldspar through reaction with plagioclase feldspar-derived Al_2O_3 and CaO yielding muscovite 2, zoisite, jadeite, and quartz. The textural evidence for this possible transformation remains ambiguous.

PROCESSES OF FORMATION OF TRANSITION ORTHOGNEISS

The well-defined planar fabric, more homogeneous phase compositions, and coarser grain size of pyroxene, garnet, and phengite, as well as the absence of biotite distinguish the transition orthogneiss from the metaquartz diorite. These textural, mineralogical, and chemical differences are the result of high-strain deformation which is therefore inferred to have greatly influenced the rates of diffusion and reaction.

The most notable characteristic of the transition orthogneiss is the intense deformation of the pyroxene-rich aggregate. Rubie (1983) has argued that deformation took place after completion of the plagioclase breakdown reactions (1) and (2), and that the small grain size of the jadeite + quartz + zoisite aggregates may have permitted deformation by a mechanism of grain boundary sliding accommodated by diffusive mass transfer. The main evidence for the operation of this mechanism is that the fine-grained, pyroxene-rich aggregates of the metaquartz diorite were more deformable than quartz (Fig. 2c), whereas medium-to coarse-grained Na-pyroxene is invariably much less deformable than quartz (Rubie, 1983, Fig. 7). Compared to the metaquartz diorite, the larger grain size of the Na-pyroxene in the transition orthogneiss indicates that grain coarsening occurred during and/or after deformation. If grain boundary sliding was the dominant deformation mechanism, synkinematic grain growth must have acted as a strain hardening process in these rocks due to the grain size sensitivity of this type of deformation mechanism (see Rubie, 1984*b*).

Deformation may have had a strong catalytic effect on the kinetics of several processes in these rocks. More favourable growth kinetics and faster diffusion rates during deformation may have been responsible for the completion of reaction (4), the accompanied grain-

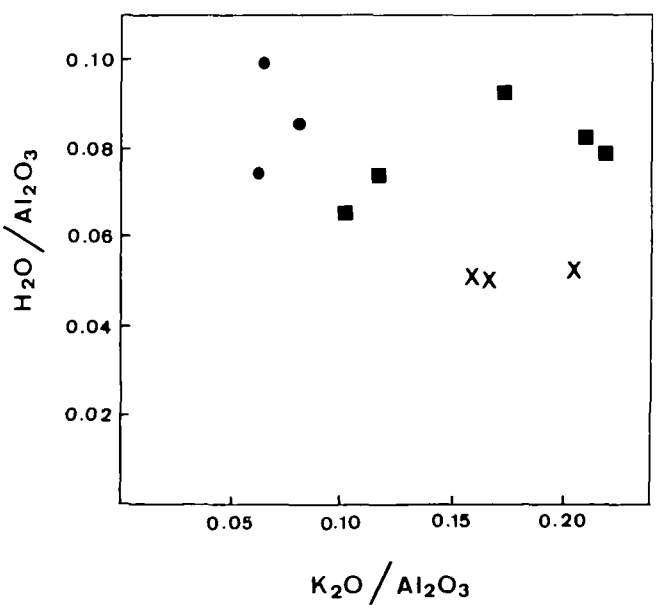

FIG. 7. Weight per cent ratios H_2O/Al_2O_3 against K_2O/Al_2O_3 for samples of metaquartz diorite (crosses), transition orthogneiss (squares) and orthogneiss (circles). H_2O and K_2O have been normalized to Al_2O_3 (see Ferry, 1983) assuming that alumina was relatively immobile during metamorphism (Carmichael, 1969; Thompson, 1975; Rubie, 1982). The data suggest that deformed samples have been slightly enriched in H_2O relative to the undeformed samples, and also that K_2O depletion has occurred (see also Table 1). A similar trend is obtained by plotting H_2O against K_2O. Systematic trends for the other major elements have not been found.

coarsening, and the chemical homogenization of the garnet and phengite. Although coarser-grained and deformed, the pyroxenes show little evidence of having approached an equilibrium composition (Fig. 4), and are therefore regarded as having been metastable during the formation of the transition orthogneiss. The failure of pyroxenes to equilibrate was presumably due to slow intracrystalline diffusion rates (cf. Freer *et al.*, 1982; Brady & McCallister, 1983)—this supports the proposed grain boundary sliding deformation mechanism because deformation mechanisms involving the movement of dislocations enhance intracrystalline diffusion rates (Yund & Tullis, 1980).

Deformation can enhance reaction kinetics in a number of ways (see Brodie & Rutter, 1985). It may enhance permeability therefore allowing infiltration of water into the system (Rutter & Brodie, 1985). The addition of even small traces of H_2O to a previously dry system can increase rates of reaction and grain coarsening by several orders of magnitude (Fyfe *et al.*, 1958, pp. 84–85; Tullis & Yund, 1982; Rubie, 1986). There is evidence for possible infiltration by at least small quantities of hydrous fluid during and/or after the high-strain deformation of the metaquartz diorite. Whole rock chemical data suggest that all deformed rocks derived from metaquartz diorite are slightly enriched in H_2O (Table 1 and Fig. 7, see also Oberhaensli *et al.*, 1985). The extent of replacement of Na-pyroxene by phengite aggregates suggests either hydration or localised redistribution of water within the rock (Fig. 2d). Isotopic evidence also suggests localised infiltration of small quantities of fluid into the deformed rocks (Frueh-Green, 1985). In addition, the veins of garnet + zoisite located along many shear zones in metaquartz diorite were presumably formed under conditions of high fluid pressure. In general these veins were post-kinematic, although synkinematic (folded) veins have also been observed.

ORTHOGNEISS-FORMING PROCESSES AND REACTIONS

As previously discussed, grain coarsening and annealing of pyroxene in the superplastically deformed layers may have caused strain hardening during the metaquartz diorite→transition orthogneiss evolution. During further deformation most of the strain was taken up by quartz and muscovite. The pyroxene-rich layers became strongly disrupted into individual pyroxenes and clusters of pyroxene which are characteristic of the orthogneiss. This microstructural reworking and subsequent grain coarsening and annealing destroyed all evidence of the earlier superplastic deformation, i.e. the main strain-producing deformation mechanism.

The decreasing jadeite content in pyroxene, partial resorption textures of the garnet, and the large modal percentage of paragonite distinguish the orthogneiss from the transition orthogneiss and metaquartz diorite. These suggest that a disequilibrium transition such as

$$\text{Jadeite} + \text{garnet} + H_2O + SiO_2 \rightarrow \text{omphacite} + \text{paragonite} \qquad \text{(Reaction 7)}$$

took place during the evolution from transition orthogneiss to orthogneiss. Undulose extinction and sub-grain boundaries in orthogneiss pyroxenes suggest that intracrystalline deformation involving the movement of dislocations occurred. This process is presumed to have enhanced intracrystalline diffusion rates and may have catalysed reaction (7). This transition also requires addition of water, as discussed above (see also Fig. 7).

REACTION HISTORY

The mineralogical characteristics which distinguish the orthogneiss from other rock types of similar bulk composition in the Sesia Zone are primarily the large variations in pyroxene

composition with a tendency for jadeitic compositions to evolve towards omphacitic compositions but with an absence of systematic zoning patterns, the high grossular content of the garnets, and the high modal proportion of paragonite. These mineralogical characteristics may be due to two different possible reaction histories. (1) The orthogneiss lies in a compositional space in which continuous reactions are responsible for the distinctive phase chemistry in a near-equilibrium environment. (2) The orthogneiss was derived from the disequilibrium mineral associations of the metaquartz diorite and kinetic factors, coupled with the deformation history, controlled an approach towards (partial) equilibrium and were responsible for the present mineralogy. Both possibilities are discussed below.

An equilibrium reaction history

A possible explanation for the variation in pyroxene composition in the orthogneiss is that an originally jadeitic pyroxene re-equilibrated towards omphacite as changes in pressure occurred. This possibility is difficult to prove and it cannot be shown, for example, that such re-equilibration occurred under conditions of decreasing pressure in the eclogite facies, during the early stages of uplift of the Sesia Zone, because evidence for equilibrium between albite and jadeite or omphacite is never observed. The only sodic pyroxene which crystallized in equilibrium with albite, under conditions of reduced pressure during uplift, is chloromelanite which occurs as a breakdown product of jadeite and omphacite (Lombardo *et al.*, 1977; Oberhaensli *et al.*, 1985).

In the absence of albite, continuous reactions involving the jadeite exchange can occur as a result of changes of pressure. For example, in Sesia Zone rocks of quartzo–feldspathic composition, in which amphibole is a major constituent phase, the zonation pattern in the pyroxenes has been shown to be due to several coupled continuous reactions (Koons, 1982, 1986). These reactions produce increasingly jadeitic pyroxenes, increasingly glaucophanitic amphiboles, and lower grossular contents in the garnets with increasing pressure. In the orthogneiss, the buffering capacity of the assemblage differs from that of the amphibole-bearing assemblages and although it is probable that continuous reactions would produce a less jadeitic pyroxene with *decreasing* pressure, the alternative possibility that a less jadeitic pyroxene will develop with *increasing* pressure cannot be excluded.

A disequilibrium reaction history

We now propose a model for the evolution of the orthogneiss in the eclogite facies, which involves disequilibrium processes. In this model, the mineralogy is dependent on the reaction pathway rather than being solely dependent on P, T and whole rock composition and is therefore a function of time and the processes which enhance or inhibit the rates of diffusion and reaction. The basis of the model is that the orthogneiss was formed by deformation of the metaquartz diorite and has inherited its distinctive mineralogical characteristics from this earlier stage of disequilibrium mineral associations.

Lombardo *et al.* (1977) have shown that the most important control on pyroxene composition during high-pressure metamorphism is the bulk rock chemistry. In most eclogitic schists, jadeite only occurs in rocks such as metagranites and meta-aplites which are low in FeO, MgO, and CaO and high in SiO_2 compared with rocks containing omphacite. There is also a strong correlation between Na/(Na + Ca) in the pyroxene and in the host rock (Fig. 8). Lombardo *et al.* (1977) have also emphasized, in support of the above conclusion, that jadeite- and omphacite-bearing rocks are closely associated in the field and show indications of having crystallized under the same P–T conditions.

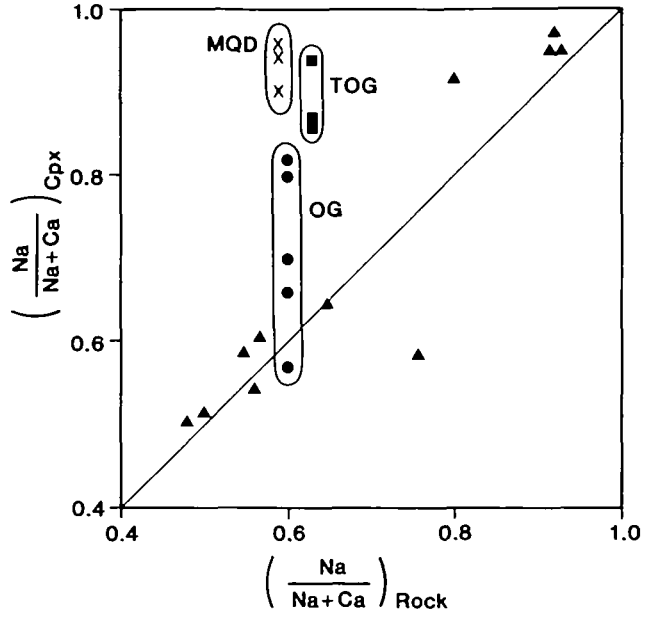

FIG. 8. Na/(Na + Ca) ratio of omphacitic and jadeitic pyroxenes plotted against Na/(Na + Ca) ratio of the host rock for eclogitic schists and gneisses from the Sesia Zone. The triangular symbols are data of Lombardo *et al.* (1977) which show a strong correlation between pyroxene composition and whole rock composition. Data for the metaquartz diorite (MQD, crosses), transition orthogneiss (TOG, squares) and orthogneiss (OG, circles) deviate significantly from this trend, as discussed in the text.

The compositions of the phases which formed in the metaquartz diorite were controlled primarily by the chemical compositions of localized domains. Although local equilibrium probably existed, there was a state of disequilibrium on the scale of a thin section between the different domains (this behaviour has been described as 'mosaic equilibrium' by some authors). Jadeitic pyroxene formed in Domain I, which originally consisted of sodic plagioclase, because the localized composition of this domain was low in FeO, MgO, and CaO and high in Na_2O. According to the data and conclusions of Lombardo *et al.* (1977), which show that omphacitic pyroxenes generally occur in eclogitic schists and gneisses of quartz diorite composition, this jadeitic pyroxene had a disequilibrium composition in terms of the whole rock chemistry and was therefore metastable (Fig. 8).

When chemical communication was increased, during deformation, equilibration between phases occurred within new and larger domains. These enlarged domains encompassed different effective bulk compositions from the individual domains of the original metaquartz diorite. However, the deformation which transformed the metaquartz diorite into the transition orthogneiss caused little shift in pyroxene compositions (for reasons discussed above). The high jadeite content and the large range of X_{Mg} values in the pyroxenes of the transition orthogneiss show that this mineral remained metastable with respect to the whole rock composition and was therefore in disequilibrium with other phases (Figs. 4 and 8). Garnet and phengite compositions homogenized during this stage. Therefore, these latter minerals are assumed to have equilibrated to the bulk composition of a new domain which, as pyroxene failed to equilibrate at this stage, may have approximated the whole rock composition minus the pyroxene component.

During subsequent deformation, which produced orthogneiss from the transition

orthogneiss, diffusion in the pyroxenes was apparently enhanced by the movement of dislocations. The composition of this mineral readjusted to a new and more mafic effective bulk composition, which may have approximated that of the whole rock, by becoming more omphacitic. Thus, in this disequilibrium model, the variation in pyroxene compositions in the orthogneiss is due to the partial equilibration of the original jadeitic pyroxene (metastable in terms of the whole rock composition) to omphacite (stable in terms of the whole rock composition) (see Fig. 8).

The reaction of jadeite to omphacite involved significant changes in X_{Mg}^{Cpx} (Fig. 4). However, although garnet resorption occurred during this reaction (reaction 7), there is no evidence from zoning profiles that the compositions of the residual garnets readjusted at this stage. Therefore, it cannot be assumed that Fe–Mg exchange equilibrium was achieved between pyroxene and garnet. The application of the garnet–clinopyroxene geothermometer of Ellis & Green (1979) confirms this point and also emphasizes the persistence of disequilibrium between garnet and pyroxene throughout the metaquartz diorite to orthogneiss evolution. Taking a range of pyroxene compositions from the metaquartz diorite together with the composition of a garnet rim in spatial proximity to Domain I (Analysis 'C', Table 4, Fig. 3) results in temperature estimates ranging from 1150 °C upwards (at 16 kb). Estimated temperatures for the transition orthogneiss, based on garnet rim compositions and a range of pyroxene compositions, lie between 770 and 1400 °C. Similarly, temperature estimates of 730–800 °C are obtained from the orthogneiss. These latter estimates are ~200 °C higher than the normally-accepted temperature estimates for the eclogite facies metamorphism in the Sesia Zone (e.g., Compagnoni, 1977) and are therefore presumed to be a consequence of disequilibrium between garnet and omphacite.

It should be emphasized that, in contrast to the metaquartz diorite, there are no obvious textural indications of disequilibrium in the transition orthogneiss or, apart from evidence of garnet resorption, in the orthogneiss. Indications of disequilibrium in the deformed rocks have resulted primarily from studying the mineralogical and microstructural evolution which provides a perspective not generally available in petrologic studies. Even physical contact between mineral grains does not necessarily indicate that they were ever in equilibrium. An example of this phenomenon occurs in contact metamorphosed emeries of the Cortlandt Complex, New York in which contacts between grains of corundum and quartz have persisted through temperature of 650–900 °C (Tracy & McLellan, 1985).

The above discussion indicates that there is considerable difficulty in defining either an equilibrium assemblage or local domains of equilibrium in the orthogneiss. This conclusion obviously has important consequences for the application of thermobarometric methods. Compositions of coexisting phases used in pressure estimates which utilize net transfer reactions reflect the pressure of metamorphism only within the constraints imposed by the buffering assemblages. If such a buffering system cannot be correctly defined, the pressure of formation of the assemblage is not independently determinable from the compositional variation within individual phases.

The timing of deformation was probably critical to the mineralogical evolution of the orthogneiss in this disequilibrium reaction history. If for example, penetrative deformation had occurred prior to the onset of metamorphic reactions such as the breakdown of plagioclase and biotite (reactions 1–6), it is possible that a state of equilibrium (on the scale of a thin section) would have been more closely approached throughout the reaction history. In that case, an equilibrium assemblage including garnet, omphacite, quartz, paragonite, phengite, and zoisite may have developed at the onset of the high pressure event with subsequent changes in P and T being recorded by zoning patterns in these minerals. However, in the case of the Monte Mucrone orthogneiss, and perhaps other Alpine

orthogneisses, disequilibrium effects preclude an evaluation of P–T paths based solely upon mineral analyses. Properties of the quartz diorite which appear to have been critical factors in the disequilibrium reaction history were a paucity of grain boundary fluid and consequently slow intracrystalline diffusion rates, a high resistance to deformation prior to the breakdown of plagioclase and a low resistance to deformation subsequent to the formation of fine-grained jadeitic pyroxene.

Finally, one uncertainty concerning the disequilibrium model is the time scale involved. Although the mineralogical evolution discussed here could have occurred under isothermal and isobaric conditions over a relatively short time period, there is also the possibility that it took place over a protracted time period during which changes in P and T played some role in controlling the mineralogy.

ACKNOWLEDGEMENTS

Alan Thompson provided the impetus for this study by suggesting that the Monte Mucrone rocks might still contain information on metamorphic evolution. Subsequent readings of different manuscripts by Alan, Volkmar Trommsdorff, Werner Schreyer, Giles Droop, Stöff Heinrich and John Ridley helped to clear a number of murky issues. Critical reviews by Martin Engi, Christian Chopin, and Gerhard Voll substantially improved the presentation of the manuscript and are greatly appreciated. We thank J. Sommerauer for assistance with microprobe analyses. The project was supported financially by Schweizerische Nationalfonds (grants 2.7720.77, 2.011–0.81 and 272010187) and the E. T. H. (grant 5.501.330.752/4).

REFERENCES

Brady, J. B., & McCallister, R. H., 1983. Diffusion data for clinopyroxenes from homogenization and self-diffusion data. *Am. Miner.* **68**, 95–105.

Brodie, K. H., & Rutter, E. H., 1985. On the relationship between deformation and metamorphism, with special reference to the behaviour of basic rocks. In: Thompson, A. B. & Rubie, D. C. (eds.) *Advances in Physical Geochemistry*, vol. 4, Metamorphic reactions: Kinetics, textures and deformation. New York: Springer–Verlag.

Carmichael, D. M., 1969. On the mechanism of prograde metamorphic reactions in quartz-bearing pelitic rocks. *Contr. Miner. Petrol.* **20**, 244–67.

Compagnoni, R., 1977. The Sesia–Lanzo Zone: high pressure-low temperature metamorphism in the Austroalpine continental margin. *Rend. Soc. Ital. Miner. Petrol.* **33**, 335–74.

—— Dal. Piaz, G. V., Hunziker, J. C., Gosso, G., Lombardo, B., & Williams, P. F., 1977. The Sesia-Lanzo Zone, a slice of continental crust with Alpine high pressure-low temperature assemblages in the Western Italian Alps. *Ibid.* **33**, 281–334.

—— Maffeo, B., 1973. Jadeite-bearing metagranitoids l.s. and related rocks in the Mount Mucrone area (Sesia-Lanzo Zone, Western Italian Alps). *Schweiz. Miner. Petrogr. Mitt.* **53**, 355–78.

Desmons, J., & Ghent, E. D., 1977. Chemistry, zonation and distribution coefficients of elements in eclogitic minerals from the eastern Sesia unit, Italian Western Alps. *Ibid.* **57**, 397–411.

de Groot, S. R., & Mazur, P., 1962. *Non-Equilibrium Thermodynamics*. Amsterdam: North Holland.

Ellis, D. J., & Green, D. H., 1979. An experimental study of the effect of Ca upon garnet–clinopyroxene Fe–Mg exchange equilibria. *Contr. Miner. Petrol.* **71**, 13–22.

Essene, E. J., & Fyfe, W. S., 1967. Omphacite in Californian metamorphic rocks. *Ibid.* **15**, 1–23.

Ferry, J. M., 1983. Regional metamorphism of the Vassalboro formation, south-central Maine, USA: a case study of the role of fluid in metamorphic petrogenesis. *J. geol. Soc. Lond.* **140**, 551–76.

Fisher, G. W., 1973. Non-equilibrium thermodynamics as a model for diffusion controlled metamorphic processes. *Am. J. Sci.* **273**, 897–924.

—— 1977. Nonequilibrium thermodynamics in metamorphism. In: Fraser, D. G. (ed.) *Thermodynamics in Geology*. Boston: Reidel, 381–403.

Foster, C. T. Jr., 1977. Mass transfer in sillimanite-bearing pelitic schists near Rangeley, Maine. *Am. Miner.* **62**, 727–46.

—— 1981. A thermodynamic model of mineral segregations in the lower sillimanite zone near Rangeley, Maine. *Ibid.* **66**, 260–77.

Freer, R., Carpenter, M. A., Long, J. V. P., & Reed, S. J. B., 1982. 'Null result' diffusion experiments with diopside: implications for pyroxene equilibria. *Earth planet. Sci. Lett.* **58,** 285–92.

Frueh-Green, G., 1985. Stable isotope indications of fluid involvement in ductile shear zones during eclogite facies metamorphism. *Trans. Am. geophys. Union* **66,** 1126–7.

Fyfe, W. S., Turner, F. J., & Verhoogen, J., 1958. Metamorphic reactions and metamorphic facies. *Geol. Soc. Am. Mem.*, 73.

Griffin, W. L., & Raheim, A., 1973. Convergent metamorphism of eclogites and dolerites, Kristiansund area, Norway. *Lithos*, **6,** 21–40.

Hy, C., 1984. Metamorphisme polyphase et evolution tectonique dans la croute continentale eclogitisee: Les series granitiques et pelitiques du Monte Mucrone (Zone Sesia–Lanzo, Alpes Italiennes). Mem. Sc. Terre Univ Curie, no. 84–51.

Joesten, R., 1977. Evolution of mineral assemblage zoning in diffusion metasomatism. *Geochim. cosmochim. Acta*, **41,** 649–70.

Katchalsky, A., & Curran, P. F., 1965. *Nonequilibrium Thermodynamics in Biophysics*. Cambridge, Mass.: Harvard University Press.

Koons, P. O., 1981. A study of natural and experimental metasomatic assemblages in an ultramafic-quartzofeldspathic system from the Haast Schist, South Island, New Zealand. *Contr. Miner. Petrol.* **78,** 189–95.

—— 1982. An investigation of experimental and natural assemblages from the Sesia Zone, Western Alps, Italy, Unpublished Dr. Sc. Nat. thesis, ETH, Zurich.

—— 1986. Relative geobarometry from high-pressure rocks of quartzofeldspathic composition from the Sesia Zone, Western Alps, Italy. *Contr. Miner. Petrol.* **93,** 322–44.

Korzhinskii, D. S., 1959. Physicochemical basis of the analysis of the paragenesis of minerals. New York: Consultants Bureau Inc, 142 pp. (English translation).

Lombardo, B., Compagnoni, R., Fiora, L., & Facchinelli, A., 1977. Composition of some sodic pyroxenes from the eclogitic mica schists of Lower Val d'Aosta (Sesia–Lanzo Zone, Western Alps). *Rend. Soc. Ital. Miner. Petrol.* **33,** 375–87.

Loomis, T. P., 1976. Irreversible reactions in high grade metapelitic rocks. *J. Petrology*, **17,** 559–88.

Mørk, M. B. E., 1985. Incomplete high *P–T* metamorphic transitions within the Kvamsoy pyroxenite complex, West Norway: a case study of disequilibrium. *J. metamorphic Geol.* **3,** 245–64

Oberhaensli, R., Hunziker, J. C., Martinotti, G., & Stern, W. B., 1982. Mucronites: an example of Eo-Alpine eclogitization of Permian granitoids, Italy. *Terra Cognita*, **2,** 325.

—— —— —— —— 1985. Monte Mucrone: an example of Eo-Alpine eclogitization of Permian granitoids, Sesia-Lanzo Zone (Western Alps). *Chem. Geol.* (Isotope Geoscience Section) **52,** 165–84.

Prigogine, I., 1967. *Introduction to Thermodynamics of Irreversible Processes*. Third Edition. New York: John Wiley.

Ridley, J., & Dixon, J. E., 1984. Reaction pathways during the progressive deformation of a blueschist metabasite: the role of chemical disequilibrium and restricted range equilibrium. *J. metamorphic Geol.* **2,** 115–28.

Rubie, D. C., 1982. Mass transfer and volume change during alkali metasomatism at Kisingiri, Western Kenya. *Lithos*, **15,** 99–109.

—— 1983. Reaction-enhanced ductility: the role of solid–solid univariant reactions in deformation of the crust and mantle. *Tectonophysics*, **96,** 331–52.

—— 1984*a*. A thermal-tectonic model for high-pressure metamorphism and deformation in the Sesia Zone, Western Alps. *J. Geol.* **92,** 21–36.

—— 1984*b*. The olivine–spinel transformation and the rheology of subducting lithosphere. *Nature*, **308,** 505–08.

—— 1986. The catalysis of mineral reactions by water and restrictions on the presence of aqueous fluid during metamorphism. *Miner. Mag.* **50,** 399–415.

Rutter, E. H., & Brodie, K. H., 1985. The permeation of water into hydrating shear zones. In: Thompson, A. B., & Rubie, D. C. (eds.) *Advances in Physical Geochemistry*, vol. 4, Metamorphic reaction: Kinetics, textures and deformation. New York: Springer-Verlag, 242–50.

Spear, F. S., Ferry, J. M., & Rumble, D. III, 1982. Analytical formulation of phase equilibria: the Gibb's method. In: Ferry, J. M. (ed.) *Reviews in Mineralogy*, vol. 10, Characterization of metamorphism through mineral equilibria. *Miner. Soc. Am.*, 105–152.

Thompson, A. B., 1975. Calc-silicate diffusion zones between marble and pelitic schist. *J. Petrology*, **16,** 314–46.

Thompson, J. B., 1959. Local equilibrium in metasomatic processes. In: Abelson, P. H. (ed.) *Researches in Geochemistry*. New York: John Wiley, 427–57.

Tracy, R. J., McLellan, E. L., 1985. A natural example of the kinetic controls of compositional and textural equilibration. In: Thompson, A. B., & Rubie, D. C. (eds.) *Advances in Physical Geochemistry*, vol. 4, Metamorphic reactions: Kinetics, textures and deformation. New York: Springer-Verlag, 118–37.

Tullis, J., & Yund, R. A., 1982. Grain growth kinetics of quartz and calcite aggregates. *J. Geol.* **90,** 301–18.

van Roermund, H., Lister, G. S., & Williams, P. F., 1979. Progressive development of quartz fabrics in a shear zone from Monte Mucrone, Sesia–Lanzo Zone, Italian Alps. *J. struct. Geol.* **1,** 43–52.

Weare, J. H., Stephens, J. R., & Eugster, H. P., 1976. Diffusion metasomatism and mineral reaction zones: general principals and application to feldspar alteration. *Am. J. Sci.* **276,** 767–816.

Yund, R. A., & Tullis, J., 1980. The effect of water, pressure, and strain on Al/Si order-disorder kinetics of feldspar. *Contr. Miner. Petrol.* **72,** 297–302.